Source Localization of Crackle-Related Events in Military Aircraft Jet Noise

Aaron B. Vaughn,* Kent L. Gee,† S. Hales Swift,‡ and Kevin M. Leete§
Brigham Young University, Provo, Utah 84602
Alan T. Wall¶
U.S. Air Force Research Laboratory, Wright–Patterson Air Force Base, Ohio 45433
and
J. Micah Downing** and Michael M. James††
Blue Ridge Research and Consulting, LLC, Asheville, North Carolina 28801

Crackle is a perceptual feature of supersonic jet noise that is related to the presence of acoustic shocks. This study investigates the apparent source locations of the steepest shocklike events in the noise field of a high-performance military jet aircraft using an event-based time-domain beamforming method. This method uses the cross correlation between adjacent microphones to determine the angle of propagation of an ensemble of shock-related events within the time waveform. This angle of propagation is then traced back toward the source to find the apparent source location. Based on the propagation angle, derivative skewness, and overall sound pressure level, the microphone positions along the array are sorted into six groups. Shock events from groups related to crackle perception in the near field originate anywhere from 2 to 14.5 m downstream along the nozzle lip line, with distributions that shift downstream and broaden with increasing engine power. The crackle-related events appear to be generated by Mach wave radiation and large-scale turbulence structure noise.

Nomenclature

D	=	jet nozzle diameter
$R_{xy}(\tau)$	=	cross-correlation function
$Sk\{\partial p/\partial t\}$	=	skewness of the pressure time derivative, "derivative skewness"
x	=	sideline distance, m
z	=	axial distance, m
$\Delta\tau$	=	cross-correlation time lag, s
θ	=	polar angle from engine inlet, deg
ρ_{xy}	=	cross-correlation coefficient
ϕ	=	offset angle of the microphone array from the jet centerline, deg
ψ	=	incidence angle to the microphone array, deg

I. Introduction

CRACKLE is an audible component of high-power jet noise previously described as annoying [1] and dominant [2]. In the initial study of crackle in supersonic commercial aircraft noise, Ffowcs Williams et al. [1] described these aircraft as "particularly prone to producing sudden spasmodic bursts of a rasping fricative sound." They further stated, "It is a startling staccato of cracks and bangs and its onomatope, 'crackle' conveys a subjectively accurate impression." Since the publication of this initial investigation,

differing definitions of crackle have emerged as various metrics [3–7] and methodologies [7–10] have been developed as part of efforts to understand its cause and characteristics. In this study, we define crackle as a perceptual feature of supersonic jet noise that is related to the reception of acoustic shocks. This is in accord with the assertion made by Ffowcs Williams et al. that the "physical feature of a sound wave that gives rise to the readily identifiable subjective impression of 'crackle' is shown to be the sharp shock-like compressive waves that sometimes occur in the waveform [1]."

Acoustic shocks are rapid pressure increases that are characterized in a recorded waveform as large positive derivatives. For shocks in supersonic jet noise, the formation, strengthening, and persistence of the shocks in the far field are largely due to nonlinear effects [11–13]. Although the far-field shock evolution is of importance to quantifying community response to flyovers at high powers, source-related investigations are also of importance because of the potential to understand noise production in a way that could provide guidance for future noise reduction methods and technologies, such as those described in Refs. [14–17].

Recent crackle-related studies have used numerical and laboratory-scale datasets to examine steepened-wave or shocklike features in and near the jet. A growing number of numerical investigations have used diverse jet conditions (e.g., nozzle pressure ratios [18], Mach numbers [19,20], and temperature ratios [21–25]) and an assortment of simulation methods to study the jet flow and subsequent noise field. Several of these numerical studies report acoustic shocks with large pressure skewness (the foundation for the original Ffowcs Williams et al. [1] criterion) values forming at or near the turbulent shear layer of the jet [19–22]. These findings are complemented by laboratory-scale jet studies that suggest the generation of impulsive signatures exists over a distributed range rather than a localized source region [26–29].

The analysis approach introduced in this paper is founded on a crackle criterion that has been tied to human subject testing [30–33]. With crackle defined as a perceptual feature, listening tests are necessary to link the human perception to measurable noise characteristics. Prior studies [30,31] used signal processing and informal listening tests to identify the skewness of the time derivative of the pressure waveform, $Sk\{\partial p/\partial t\}$ (or derivative skewness), as a measure for the crackle percept. Recently, a relationship between derivative skewness and crackle has been quantified in the first formal jury-based listening study of crackle [32,33]. The study employed F-35A waveforms with

*Graduate Student, Department of Physics and Astronomy.
†Professor, Department of Physics and Astronomy. Senior Member AIAA.
‡Postdoctoral Research Associate, Department of Physics and Astronomy. Member AIAA.
§Graduate Student, Department of Physics and Astronomy. Student Member AIAA.
¶Research Physicist, Battlespace Acoustics Branch.
**President and Chief Scientist. Member AIAA.
††Senior Vice President and Chief Engineer. Member AIAA.

various degrees of *crackliness* [32] and a range of values for both pressure skewness and derivative skewness. A total of 31 participants auralized the waveforms as part of a category subdivision scaling test [32] and rank ordered them in a complementary exercise [33]. The subdivision scaling test resulted in a model for five crackliness categories (smooth noise, rough noise, intermittent crackle, continuous crackle, and intense crackle) based on derivative skewness, whereas the relationship between pressure skewness and the crackle percept was found to be statistically insignificant [32]. The listening test revealed that a jet noise waveform with a $Sk\{\partial p/\partial t\} > 3$ is perceived to "continuously crackle." This criterion is used as part of the analysis reported herein.

To find the regions in the jet responsible for crackle-containing waveforms in the field, this study examines the origins of waveform segments chosen by the presence of large positive derivatives that contribute significantly to the overall derivative skewness value. The origins of these waveform segments are calculated by a two-point cross-correlation beamforming method. A brief summary of the acoustical measurement of the F-35B high-performance military aircraft is provided, which is acoustically similar to the F-35A used in the subjective listener study [34]. A description of the methodology used in the beamforming process is subsequently provided. Results for four engine conditions are then discussed, which are followed by an analysis involving microphone pair groupings to describe jet noise characteristics associated with jet crackle.

II. Measurement

Acoustic pressure waveforms were collected from a static F-35B operating at several engine conditions, from 25 to 150% engine thrust request (ETR). Engine conditions greater than 100% ETR are due to the addition of afterburner. Although a much more extensive measurement array was present [34], this paper focuses on data acquired from a 71-element linear ground array. This array, which was located approximately 8–10 m from the estimated jet shear layer, is shown in Fig. 1. It consisted of GRAS 6.35 mm (1/4 in.) type 1 microphones, which spanned 32 m with a 0.45 m (18 in.) intermicrophone spacing. The pressure waveforms were synchronously acquired with National Instruments PXI-449X cards sampling at 204.8 kHz. Time waveforms were at least 27 s long for all engine conditions, except for 130% ETR, which was only 10 s in length. Jet inlet angles were defined for each microphone location relative to the microphone array reference point (MARP), which was set to 7.5 m downstream of the nozzle exit plane to be consistent with prior measurements. The nominal exit diameter of the jet engine nozzle is 1 m. Other analyses of this array are reported on in Refs. [35–39].

III. Methods

This paper employs an event-based beamforming method involving a cross correlation of adjacent microphones' waveforms windowed around particular events, from which the radiation angle and apparent origin of the events are calculated. The analysis method, which builds off of that described by Vaughn et al. [39], also resembles the method used in Refs. [28,29,40] to detect the apparent acoustic origins along the jet axis of large-amplitude events for both laboratory- and full-scale jets. The previous study by Vaughn et al. [39] examined three types of event triggers: maximum pressure values, maximum derivative values and, as a control, regularly spaced, nonoverlapping waveform segments. However, only the maximum derivative events are considered in the present analysis: for two reasons. First, the three types of event definitions revealed similar source characteristics because high-amplitude events were correlated with high-derivative events, and even relatively short event windows typically contained a high-derivative or high-amplitude event within the regularly spaced segments. Second, as demonstrated in Sec. III.A, the large-derivative values are directly linked to elevated derivative skewness, which in turn is directly correlated with the crackle percept as quantified by Gee et al. [32] and Russavage et al. [33]. The relationship between the large-derivative event trigger and derivative skewness is elaborated on in the following section.

A. Event Selection Method

Two short F-35B waveform segments with and without acoustic shocks are shown in Fig. 2. Each 10 ms waveform was taken from a measurement of the F-35B operating at maximum afterburner (150% ETR), with Fig. 2a measured at the farthest upstream microphone and Fig. 2c in the region of maximum radiation. Distinct acoustic shocks are present in Fig. 2c, which are characterized by sudden pressure increases followed by longer rarefactions. Corresponding derivatives of these waveforms are presented in Figs. 2b and 2d, with the peaks in
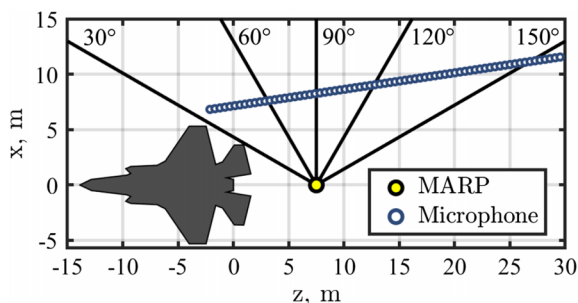

Fig. 1 Measurement schematic of the F-35B and 71-element linear ground array. Inlet angles are defined relative to the microphone array reference point.
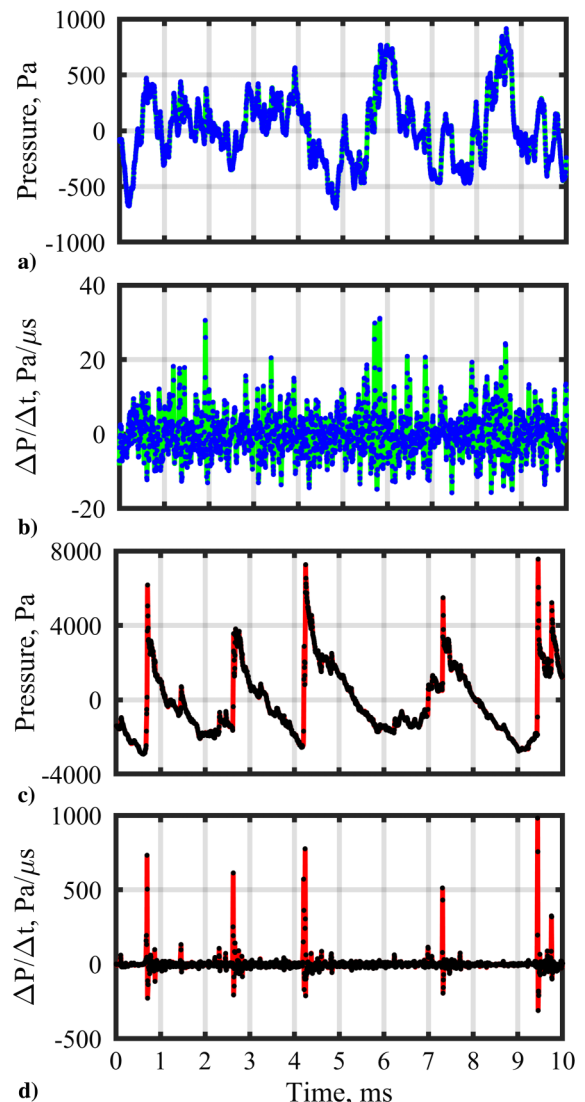

Fig. 2 Waveforms a) without and c) with acoustic shocks present, and their corresponding derivatives in Figs. 2b and 2d.

these plots corresponding to sudden increases in pressure. Based on Gee et al.'s [32] crackle criteria, the waveform represented by the segment in Fig. 2a ($Sk\{\partial p/\partial t\} = 0.6$) is considered to not contain crackle and the waveform represented in Fig. 2c ($Sk\{\partial p/\partial t\} = 9.4$) would contain "intense crackle." Auralization of the waveforms with studio-quality Sennheiser HD 650 headphones confirms the predicted crackle perception of these waveforms.

The event-based beamforming approach in this study triggers off of large derivatives, which are related to crackle via the $Sk\{\partial p/\partial t\}$. The relationship between the discretely measured pressure derivative, $\Delta p/\Delta t$, and $Sk\{\partial p/\partial t\}$ is shown in Fig. 3 with the time derivative of a 10 s pressure waveform in blue; the running $Sk\{\partial p/\partial t\}$ value calculated for nonoverlapping 20 ms segments in red; and the $Sk\{\partial p/\partial t\}$ value for the entire waveform of 3.6 in green. Large peaks in the $\Delta p/\Delta t$ waveform represent high-derivative events, and the largest $Sk\{\partial p/\partial t\}$ values occurring simultaneously with the $\Delta p/\Delta t$ peaks indicate that these events contribute most significantly to the overall $Sk\{\partial p/\partial t\}$ value of the waveform. Using this direct link of $Sk\{\partial p/\partial t\}$ with the large-derivative events in conjunction with the result of the prior subjective studies [32,33], the maximum derivative events are used in the subsequently described event-based beamforming method.

For every pair of adjacent microphones along the array, the events are selected in the upstream microphone. In the 27 s waveforms, the derivative values were sorted in descending order, and the steepest 1000 events were selected with the condition that they were not within 2.4 ms of each other to allow for distinction between shock events in the applied signal processing method. An example of a defined event is indicated by the red × in Fig. 4a. Events defined in reference channel may or may not become events in the adjacent channel when the adjacent channel is used as a reference channel for the next microphone pair because this depends upon a given large-derivative event persisting across multiple microphones. For example, the acoustic shock that occurs at about 8.5 ms in the reference channel in Fig. 4a is seen as having a significantly reduced amplitude at about 9 ms in the adjacent channel in Fig. 4b. Fievet et al. [5] observed that not all waves propagate in the same direction with the possibility of crossing waves; however, events examined in this study are observed to be related to far-field measurements [41], suggesting that potential near-field nonlinear wage merging occurs before arriving at the array. Although resulting beamformed angles may be the aggregate of merged waves, further investigation is needed to understand to what extent nonlinear merging of near-field shocklike waves occurs for military aircraft jet noise and why particular acoustic shocks change drastically between adjacent microphones.

B. Beamforming Method

After events are defined, a window is applied around each event in both the reference and adjacent channels, as shown in Fig. 4. The window is centered about the defined event in the reference channel, but when applied to the other channel in the pair, a time lag is added so that the peak of the window is at an approximation of the event in the adjacent channel. This time lag is determined by assuming the MARP
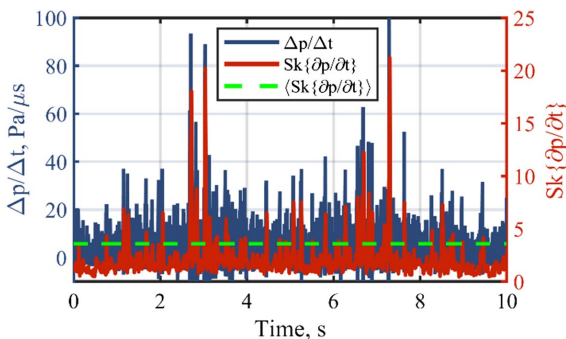

Fig. 3 Pressure waveform time derivative, $Sk\{\partial p/\partial t\}$ values calculated for every 20 ms segment, and time-averaged $Sk\{\partial p/\partial t\}$ from a 10 s waveform.
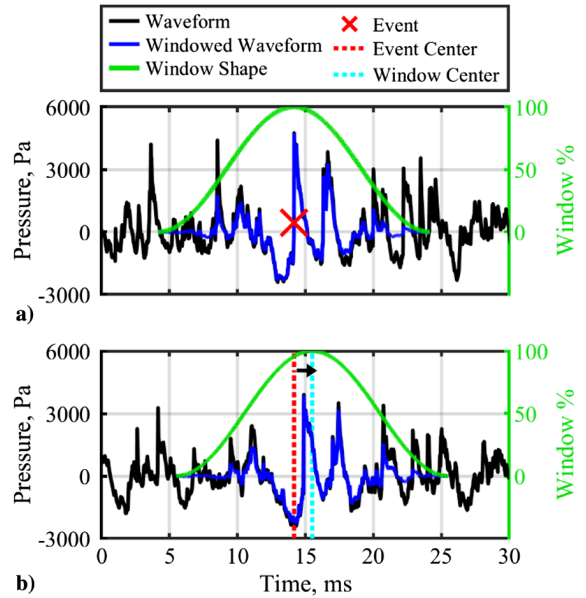

Fig. 4 Two 30 ms waveforms illustrating the application of a Hann window around a high-derivative event in a) the reference channel and the offset from the event, and b) the adjacent channel.

as the source location for the event, determining the relative path length differences, and assuming the events travel at the ambient speed of sound. A 20 ms Hann window was chosen to be sufficiently long that if the event in the adjacent channel does not line up in the center of the window, there is still enough information in the corresponding event to compute a meaningful cross correlation. Due to the length of the window, two events may overlap. However, most (greater than 90%) events occur at least 5 ms from the next closest event, where the window drops by 50%, and so most of the information captured by the different waveform segments can be considered independent of the others.

To obtain the apparent origin for each pair of windowed waveforms, a simple cross correlation is used as a time-domain beamformer. Following notation similar to that outlined by Bendat and Piersol [42], the time delay $\Delta \tau$ is calculated as follows:

$$\Delta \tau = \arg \max(R_{xy}(\tau)) \tag{1}$$

where

$$R_{xy}(\tau) = E[p_i(t)p_{i+1}(t + \tau)] \tag{2}$$

and $p_i(t)$ and $p_{i+1}(t)$ are the windowed waveforms (as exemplified in Fig. 4) from, respectively. the reference (upstream) and adjacent (downstream) channels (or microphones 1 and 2 in Fig. 5) for the ith microphone pair. Given the intermicrophone spacing and distance from the jet nozzle lip line to the array, the shock waves in the vicinity of the microphones can be considered locally planar, which simplifies the propagation angle calculation. This is justified by accounting for spherical spreading from the MARP and looking at the difference between curved and planar wave fronts; inclusion of curved wave fronts yields an angular and spatial difference of less than 0.01 deg or 0.1 mm. Assuming the shock waves are travelling at the ambient speed of sound c, a distance of $c \cdot \Delta \tau$ is found to form a right angle between the arrival path to the downstream microphone and the wave front in contact with the upstream microphone. This creates a right triangle that can be used to solve for the angle of incidence ψ in terms of $c \cdot \Delta \tau$ and the interelement spacing along the array d. The array offset angle ϕ (shown in Fig. 5) is then directly computed from the difference in the microphone locations, and then ϕ and ψ are used to compute the directivity of the event in terms of the jet inlet angle:
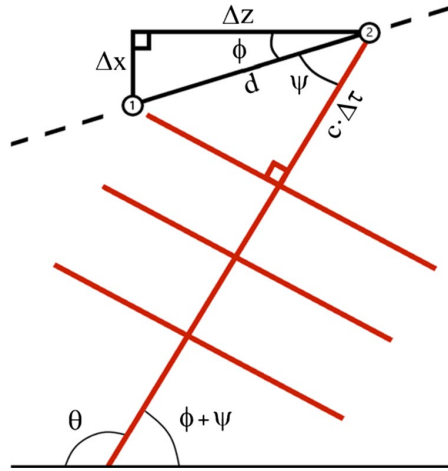
Fig. 5 Schematic depicting the adjacent two-microphone cross-correlation beamforming method.

$$\theta = 180 \ \deg - [\psi + \phi]$$

$$= 180 \ \deg - \left[\cos^{-1}\left(\frac{c \cdot \Delta\tau}{d}\right) + \tan^{-1}\left(\frac{\Delta x}{\Delta z}\right) \right] \quad (3)$$

Tracing the incident angle back to the nozzle lip line gives an apparent source location of the flow corresponding to the event. While the nozzle center is approximately 2 m off the ground, vertical information cannot be achieved from the locally planar assumption and two-point cross-correlation method; therefore, apparent origin results are limited to the downstream distance along the nozzle lip line. Each apparent source location and directivity angle found for each of the 1000 events are then compiled into normalized histograms. The process is repeated for each microphone pair in the array.

IV. Event-Based Beamforming Results

The event-based beamforming process described earlier in this paper has been applied to the F-35B for engine conditions between 75 and 150% ETR, which have far-field $Sk\{\partial p/\partial t\}$ values sufficient for the perception of continuous crackle at many angles [32,34]. Section IV.A presents normalized histograms of the propagation angle and apparent origin of the highest 1000 derivative events beamformed from microphone pairs along the ground array for 75 and 150% ETR. Additional comparisons across all four engine conditions are made in Sec IV.B.

A. Normalized Histograms

The occurrences of beamformed directivity angles are shown for 75 and 150% ETR in Fig. 6. The abscissa is the z coordinate of the microphones in the array pictured in Fig. 1, and the ordinate is the array of histogram bins (representing inlet angle in 1 deg increments). Each vertical slice of the colormap corresponds to a normalized histogram of computed angles for a microphone pair, where the histogram counts are divided by the total number of events and represented as probabilities that sum to one for each distribution. The horizontal width is the z distance between microphones in a pair. Each histogram is bounded by its 5th and 95th percentiles, and probabilities below 0.01 are set to white to emphasize the dominant trends. The transition from upstream ($\theta < 90$ deg) to downstream ($\theta > 90$ deg) radiation is shown by the dashed horizontal line at 90 deg.

For both 75 and 150% ETR, there is a distinct separation in the peak between 3 and 5 m along the array, where the directivity angle of the maximum derivative events changes from upstream to downstream radiation. This transition occurs farther downstream and is more distinct for 150% ETR. Microphone pairs located beyond 4 m for 75% ETR and 4.5 m for 150% ETR all record propagation angles greater than 90 deg, indicating aft radiation from the origin of the sound in the jet. For 75% ETR, propagation angles increase quickly at
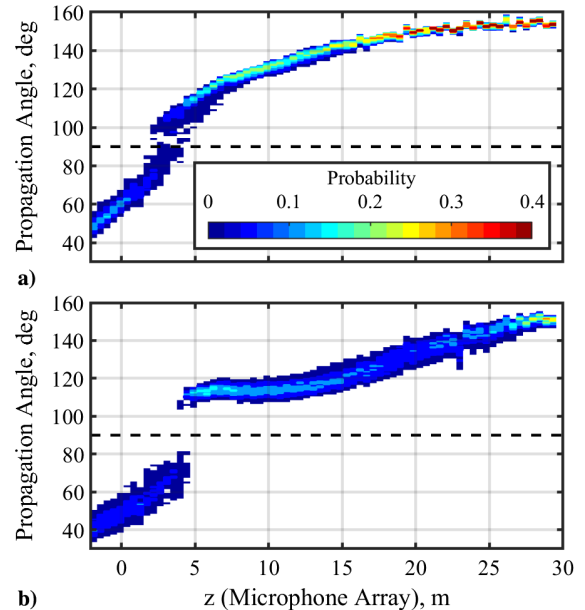

Fig. 6 Normalized histograms of propagation angle occurrence across each microphone pair for a) 75 and b) 150% ETR.

first, and then they nearly level off at the end of the microphone array; whereas for 150% ETR, the propagation angles remain constant until about 13 m before increasing to the end of the array. At the end of the microphone array, the propagation angles converge to 155 deg for 75% ETR and 150 deg for 150% ETR. These propagation angles along the microphone array when traced to the jet lip line yield an apparent origin of these steepest-derivative events.

The propagation angles, such as those in Fig. 6, are now used to ray trace the apparent origins of these high-derivative events at all four engine conditions of interest. The resulting apparent origins are compiled into normalized histograms along $x = 0.5$ m (approximately the jet nozzle lip line) and shown in Fig. 7 for 75 and 150% ETR. The abscissa is the z coordinate of the microphones, which is the same as in Fig. 6; whereas the ordinate now represents the histograms of the apparent origin along the lip line in 0.5 m bins.

The apparent origins corresponding to the upstream radiating steepest-derivative events are shown by the farthest upstream microphone pairs in Fig. 7. These events appear to originate from 2 to 5 m
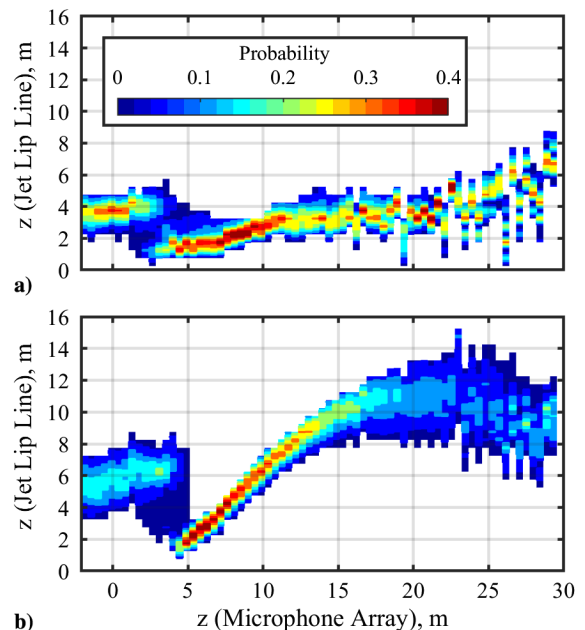

Fig. 7 Normalized histograms of apparent origin occurrence along the jet lip line across each microphone pair for a) 75 and b) 150% ETR.

Downloaded by BRIGHAM YOUNG UNIVERSITY on June 21, 2021 | http://arc.aiaa.org | DOI: 10.2514/1.J059823

downstream of the nozzle for 75% ETR in Fig. 7a and slightly farther downstream from 3 to 8 m for 150% ETR in Fig. 7b. Continuing down the microphone array, the source region broadens as the radiation transitions from forward to aft. Then, the microphones between 4 and 12 m downstream for 75% ETR and 4.5 and 14 m for 150% localize the sources of the events to compact histograms, which shift downstream. Downstream of this region, the histograms continue to shift downstream slightly and broaden. For 75% ETR, the histograms become spatially less continuous because neighboring microphone pairs do not record many counts in adjacent apparent origin bins. In contrast, at 150% ETR, the mode for each microphone pair shifts slightly downstream until about 20 m, where the now broad distribution begins to move back upstream along the lip line. This last result indicates that the events creating the largest derivatives present at the far-aft portion of the microphone array at maximum afterburner do not originate from a corresponding far-aft position. Distributions of cross-correlation coefficients are given in the Appendix and provide insight into the correlation of beamformed events.

B. Normalized Histogram Mode Comparison Across Engine Condition

Simplifying the results in Figs. 6 and 7 allows for ease of examining trends across engine power for propagation angles and apparent origins. Each histogram is reduced to its mode (with a 1 deg or 0.5 m resolution) and are shown in Fig. 8. While both the mode and mean show similar trends, the mode better represents the dominant trend in the transition region from upstream to downstream propagation, where there is not a smoothly varying transition but a bimodal distribution. The inclusion of 100 and 130% ETR demonstrates intermediate cases for the previously analyzed 75 and 150% ETR.

While exhibiting similar features across engine conditions, notable differences exist. At the farthest upstream microphone locations, the propagation angle decreases with increased engine condition, making the apparent origin shift downstream. The transition region from upstream to downstream propagation occurs farther downstream along the microphone array for higher engine conditions. Beyond the transition region along the array, higher engine conditions continue to have decreased angle or increased apparent origin, although the amount varies along the array. Immediately downstream of the transition region, minimal change in propagation angle is experienced at engine conditions greater than 75% ETR, with the region persisting over a greater span for higher engine conditions. This corresponds to
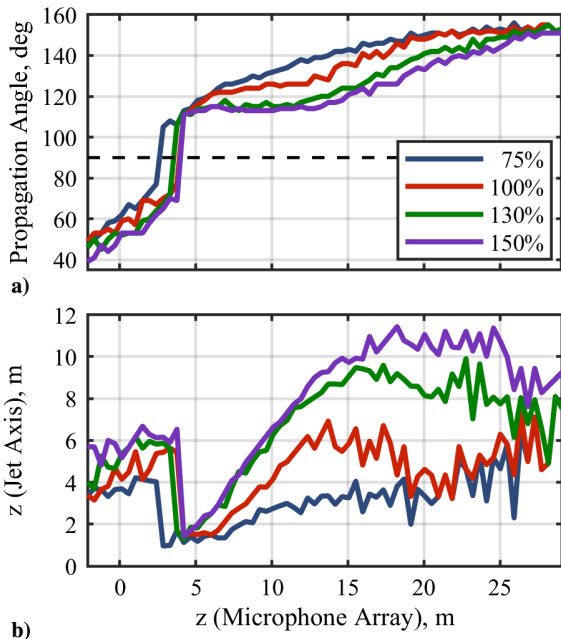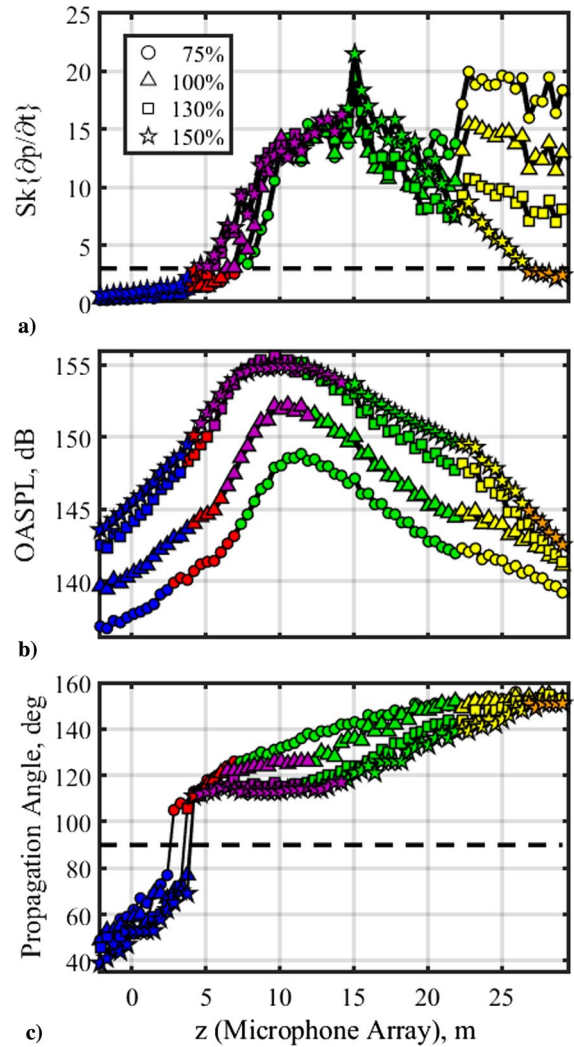

Fig. 9 Color groupings as defined in Table 1 across engine conditions for a) derivative skewness ($Sk\{\partial p/\partial t\}$), b) OASPL, and c) propagation angle along the microphone array.

the steady increase in lip-line origin in Fig. 8b from 4 to 15 m. Above 75% ETR, while maintaining downstream propagation, an inflection point where the apparent origin along the lip line transitions from an upward to a downward slope is shown in Fig. 8b at about 15 m for 100% ETR, 17 m for 130% ETR, and 25 m for 150% ETR. Beyond this region for 100% ETR, propagation angles increase to be nearly identical to 75% ETR from 19 m to the end of the array, yielding similar apparent origins. At 130% ETR, from $z = 27$ m to the end of the array is nearly identical to lower engine conditions, and while 150% ETR does decrease, it does not match those of lower engine conditions. This trend at the end of the array is interesting to note because the $Sk\{\partial p/\partial t\}$ values seen in Fig. 9 vary greatly in this region where propagation angles and apparent origins are similar.

V. Analysis

To better identify source regions important to crackle perception in the field, microphone pairs are sorted into groups using criteria suggested in Sec. V.A. The criteria used include the propagation angles found through the event-based beamforming, the measured $Sk\{\partial p/\partial t\}$, and measured overall sound pressure level (OASPL). The groupings are then assigned a color for distinction and examined graphically. Normalized histograms of the apparent origins calculated from the compilation of all microphone pairs for each group are presented and compared with other similar studies in Sec. V.C, followed by a discussion in Sec. V.D of potential jet noise phenomena associated with crackle.

Fig. 8 Comparison across ETR of the normalized histogram mode along the microphone array for a) propagation angle and b) apparent origin.

A. Microphone Pair Groupings

For each engine condition, microphone pairs are placed into one of six groups in order to correlate beamforming results with jet noise phenomena. The grouping criteria build on previously developed criteria for four groups used to analyze 75% ETR in Ref. [39]. The criteria for those four groups plus the two additionally established groups in this study are displayed in Table 1. Criteria are defined using trends in the beamformed angle of the derivative events as well as the $Sk\{\partial p/\partial t\}$ and OASPL measured at the reference microphone within the pair. The first criterion for categorizing the microphone pairs is whether the radiation direction is upstream (less than 90 deg) or downstream (greater than 90 deg) from the source to the array and whether or not the directionality is changing along the array or is unidirectional (which is defined as less than 2 deg changes compared to adjacent microphones pairs for the purposes of this work, denoted by less than $\Delta 2$ deg), as determined by the mode of the beamformed propagation angles. The second criterion is whether or not the $Sk\{\partial p/\partial t\}$ is greater or less than three, indicating that continuous crackle would be perceived by an observer at the array [32]. It should be noted that the relationship of $Sk\{\partial p/\partial t\}$ to crackle perception in Ref. [32] was made using far-field data from the 305 m arc. The $Sk\{\partial p/\partial t\}$ is expected to continue to grow beyond the array due to nonlinear propagation by as much as 1000% at 75% ETR from near the shear layer to 38 m [43]. The final criterion for group distinction is whether or not the microphone pair is upstream, downstream, or in the vicinity of a peak in the OASPL measured along the array. The first, primary peak is at about 10 m; and the second, lower peak is just beyond 22 m along the array, which may be related to the multilobe phenomenon observed in jet noise [35,36]. Application of these criteria to the microphone pairs for each of the four engine conditions generates six distinct groups. The associated jet noise phenomena given in Table 1 are discussed in Sec. V.D.

Groups are numbered by their occurrence from upstream to downstream along the microphone array. Each adjacent group generally shares one or two common criteria, as each trend for the most part is smoothly varying along the array. One abrupt trend is in propagation angle and is exemplified by upstream propagation from source to array of group 1 (blue), which is easily distinguished from all the other groups that display downstream propagation. With their primary difference in propagation angle, groups 1 and 2 (blue and red) both are not considered to continuously crackle and have low OASPLs that are spatially located upstream of the first OASPL peak. Groups 3–5 (purple, green, and yellow) all exceed the threshold at the array for continuous crackle perception. Whereas both groups 3 and 4 (purple and green) propagate downstream and are part of the first peak in the OASPL, distinction between them is the unidirectional radiation of group 3 (purple), defined by less than a 2 deg change in propagation angle between adjacent microphone pairs. Group 5 (yellow) differs from group 4 (green) by appearing in the second OASPL peak with its accompanying abrupt change in $Sk\{\partial p/\partial t\}$ at the lower engine powers. The spatial relation to the OASPL peaks is also used to differentiate group 2 (red), which occurs upstream of the first OASPL peak, from group 6 (orange) that is found downstream of the second OASPL peak at the end of the array.

The three criteria are plotted along the microphone array for 75, 100, 130, and 150% ETR in Fig. 9. Engine conditions are noted by marker, whereas colors signify the group classification as noted in Table 1. This allows for comparison of criteria across group and engine condition. The $Sk\{\partial p/\partial t\}$ shown in Fig. 9a increases slightly with increased engine power and yields a similar trend across all engine conditions up to 22 m along the array; at which point, the $Sk\{\partial p/\partial t\}$ diverges with greater values at lower engine conditions. It is curious that $Sk\{\partial p/\partial t\}$ increases with lower OASPL at lower engine conditions at the end of the array. Previously made spatial $Sk\{\partial p/\partial t\}$ maps by James et al. [34] from data collected at off-ground microphone arcs for the same F-35 measurement and by Gee et al. [43] for an earlier F-35 dataset show that $Sk\{\partial p/\partial t\}$ generally decreases with downstream distance after peaking, as is seen with 150% ETR in Fig. 9a. In comparison, it is noted that the $Sk\{\partial p/\partial t\}$ values measured at the ground array in this study are higher than at nearby off-ground microphone locations reported in Ref. [34]. A possible cause for increased $Sk\{\partial p/\partial t\}$ values at the ground is nonlinear reflections of shocks causing a greater than doubling of pressure for shock events while the remainder of the waveform reflects linearly, causing a net increase in the shock components to the waveform [41,44,45]. Further investigation into these phenomena should lend insight into understanding crackle and measurement considerations for $Sk\{\partial p/\partial t\}$.

Unlike the $Sk\{\partial p/\partial t\}$ with a diverging trend at the end of the array, the OASPL is more smoothly varying across the array for each engine condition. The OASPL is shown in Fig. 9b as a function of downstream distance along the array and has a consistent trend across engine conditions. The main peak in the OASPL occurs at 10 m and a second, smaller peak occurs at 22 m. Levels increase with engine condition, except about the main peak where the levels decrease slightly from 130 to 150% ETR. The first peak shifts slightly upstream and broadens with engine power, whereas the second peak occurs at the same location but with a steeper rolloff toward the end of the array at higher engine conditions. Although the levels plotted in Fig. 9 are directly computed from the data, the second peak in the OASPL is more pronounced when the levels are spatially normalized to a common reference distance relative to the MARP, as seen in Ref. [39], and is associated with the region with higher $Sk\{\partial p/\partial t\}$ at lower engine conditions.

B. Group Source Regions

Source regions for groups defined in Sec. V.A are found via the propagation angles of the beamformed events. The modes of the angle distribution for each microphone pair are used to draw a line from the array back to the nozzle lip line to create a visual representation of the event-based beamforming results in Fig. 10. These traced lines are color coded to represent their grouping and are shown for each engine condition with a schematic of the F-35, the nozzle lip line, the approximate location of the shear layer, and the array location. Also depicted in Fig. 10 below the jet axis are lines summarizing the region where all the events associated from that group originate. The extent represents the 5th and 95th percentile bounds, and the diamond marker notes the location of the mean with values noted in Table A1.

The upstream radiation of group 1 (blue) intersects at the nozzle lip line in the same region as groups 3 and 4 (purple and green), although there is less intersection with group 4 (green) at higher engine conditions. Group 2 (red) originates farthest upstream and has a broad overall source region. Group 3 (purple) starting at 100% ETR (see Fig. 10b) has parallel rays that persist over a broad range for both microphone pairs and the apparent source region, which increases with engine condition. When compared to group 3 (purple), the rays for group 4 (green) converge to a more localized source region, which is primarily downstream of the apparent origin of group 3 (purple) for engine conditions greater than

Table 1 Number, color, the three criteria, and jet noise phenomenon associated with each of the six microphone pair groups

| Group no.	Color	Angle, deg	$Sk\{\partial p/\partial t\}$	OASPL	Likely associated jet noise phenomenon
1	Blue	<90	<3	Upstream	Broadband shock-associated noise
2	Red	>90	<3	Upstream	Fine-scale turbulent structure noise
3	Purple	<$\Delta 2$	>3	First peak	Mach wave radiation
4	Green	>90	>3	First peak	Large-scale turbulent structure noise
5	Yellow	>90	>3	Second peak	Large-scale turbulent structure noise
6	Orange	>90	<3	Downstream	Large-scale turbulent structure noise
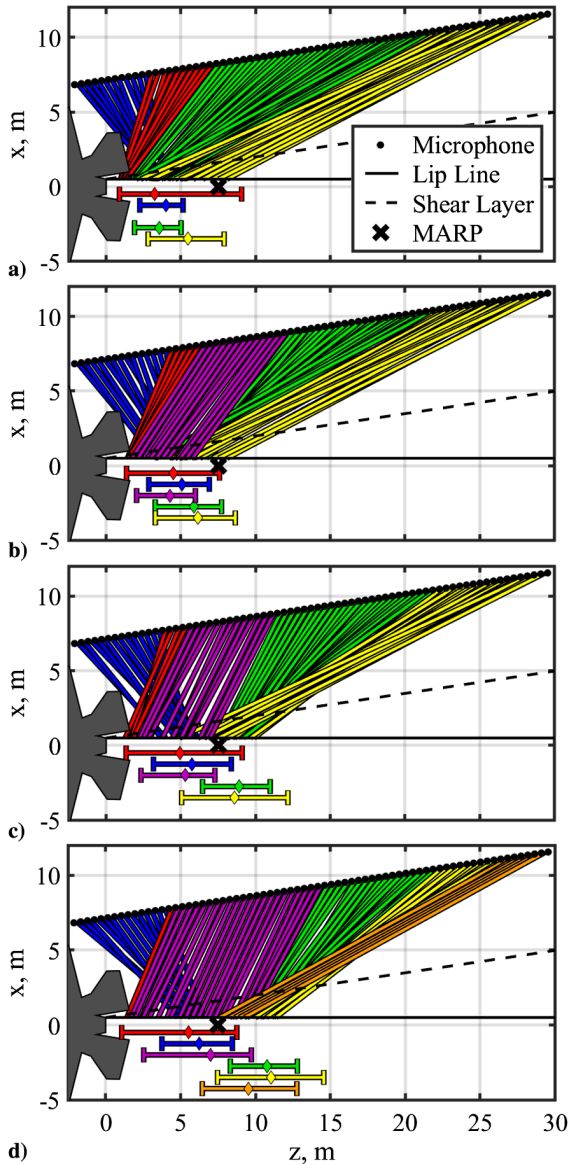
Fig. 10 Ray tracings of angle mode for each microphone pairing for a) 75, b) 100, c) 130, and d) 150% ETR. Color bounds below lip line denote the 5th and 95th percentiles with mean shown as a diamond for compiled distribution for each group with values noted in Table A1.

Fig. 11 Normalized histograms of apparent origin along nozzle lip line for all events associated with each group (colored) as well as all events (black) for a) 75, b) 100, c) 130, and d) 150% ETR. Vertical dotted line indicates MARP location.

75% ETR. Group 5 (yellow) has a similar source region as group 4 (green) with the rays farthest downstream along the array crossing over other rays to upstream locations. This crossover behavior is also exemplified by group 6 (orange) at 150% ETR.

C. Normalized Group Histograms

Distributions of the apparent origins for all the individual events associated with each group are compiled into normalized histograms in Fig. 11. Despite each group sharing similar angular, $Sk\{\partial p/\partial t\}$, and OASPL trends across engine conditions, their apparent origins primarily shift downstream as the engine condition is increased. The distribution for group 1 (blue) broadens slightly and shifts downstream with the mode increasing from about 4 to 6 m with increased engine power. Group 2 (red) maintains a peak at less than 2 m downstream of the nozzle with the increased engine condition but has a more pronounced bimodal distribution. The portion of the distribution downstream of 3 m for group 2 (red) overlaps with the distribution of group 1 (blue) that radiates upstream. Group 3's (purple) distribution shifts downstream and broadens significantly due to the unidirectional radiation persisting over a greater range with the increased engine condition. Group 4 (green) is consistently downstream of group 3 (purple), maintains a more consistent distribution width,
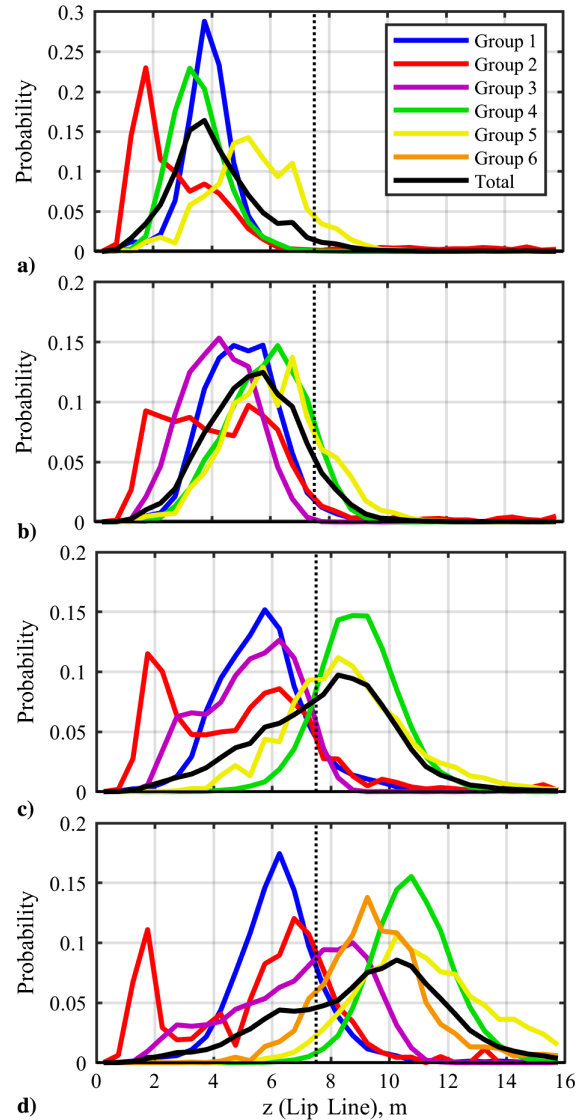
and shifts downstream with engine condition. Group 5 (yellow) has a broader source region than group 4 (green), shifts slightly downstream, and broadens with the increasing engine condition. However, due to the crossing over of the rays shown in Fig. 10, there are source regions for group 5 (yellow) at the jet lip line that are upstream of group 4 (green), as is again demonstrated by group 6 (orange). The total (black) distribution peak is most closely followed by groups 3 and 4 (green and yellow) because a larger number of microphone pairs are associated with these groups and their source regions along the lip-line overlap. This trend of source distributions broadening and shifting downstream with increased engine power is consistent with observations of general jet noise trends at all scales and matches the understanding of the stretching of the potential core of the jet with increasing Mach number [26,38,46].

The motivation for this study is to investigate the origin of crackle-related events in the near field. Examination of the histograms of the origins of the crackle-related groups (groups 3–5, where $Sk\{\partial p/\partial t\} > 3$) in Fig. 11 combined together show that the corresponding large-derivative events originate at $z = 1.9$–7.9 m along the jet lip line for 75% ETR, $z = 2.0$–8.6 m for 100% ETR, $z = 2.3$–12.2 m for 130% ETR, and $z = 2.5$–14.6 m for 150% ETR, as reported in Table A1. The sum of the crackle-related groups mirrors the overall distribution shown in black, which originates several diameters downstream of the nozzle. This is consistent with the idea

that most of the acoustic energy originates from between the potential and supersonic cores [47–49]. Because parameters such as the Mach number and temperature of the jet are unknown to the authors, the exact potential core length is unknown; however, inferences can be made from previous studies of high-performance military aircraft [38,46] and laboratory-scale jets [50]. Holography results from using the present dataset indicate a peak acoustic source region at maximum afterburner of $z = 5$–$15 D$ [38], which corresponds well with the intensity results of another aircraft at $z = 6$–$15 D$ [46]. Recent coherence analysis of a large-eddy simulation of a laboratory-scale jet operating at a temperature ratio of seven (to be on the order of a military aircraft operating at afterburner) [50] gives a source region of $z = 4$–$17 D$ and a potential core length of $7.2 D$. With $D \cong 1$ for the present aircraft, and having a comparable source region, the MARP at $z = 7.5$ m seems to be a reasonable estimate for the end of the potential core at afterburner. Given the origin of the groups relative to the end of the potential core, source mechanisms responsible for the differing groups, specifically those related to crackle, can be inferred.

D. Jet Noise Characterization

In addition to determining the source region of crackle-related events, the characteristics of microphone pair groupings created in Sec. V.A help relate groups with particular jet noise phenomena, as noted in Table 1. The non-crackle-related groups are discussed first. The upstream propagation of group 1 (blue) is likely associated with broadband shock-associated noise (BBSAN), which propagates upstream and is a dominant noise component at these locations in recent spectral characterizations [37]. Furthermore, for this F-35B measurement, holographic reconstructions of the field in Ref. [38] show the directivity and source location of the BBSAN peak, which correspond well to those of group 1 (blue), as given in Tables A1 and A2. Group 2 (red) also appears partly associated with BBSAN because its source region partly overlaps with group 1 (blue), and perhaps, with its broad source distribution and low correlation values (see Fig. A1), it is also related to fine-scale turbulence structure noise [47,51].

Examination of the individual crackle-related groups provides insight into different jet noise source phenomena. While both groups 3 and 4 (purple and green) are related to the first OASPL peak measured along the array, group 3 (purple) is characterized by a nearly constant radiation angle, consistent with the description of Mach wave radiation [10]. Groups 3, 4, and 5 (purple, green, and yellow) share a similar source region at 100% ETR; but, with the addition of afterburner, the source regions shift and separate from one another. Group 3 (purple) at afterburner originates primarily upstream of the MARP (and likely upstream of the end of the potential core), whereas groups 4 and 5 (green and yellow) originate farther downstream.

The aft radiation originating from multiple source regions is also observed in the large-eddy simulation analyzed by Leete et al. [50]. The far-aft low-frequency radiation originated from an extended area surrounding the end of the supersonic core, whereas the peak aft radiation primarily originated from the potential core region. This overall trend is also observed by Schmidt and Schmid [52], who did spectral proper orthogonal decompositions of subsonic, transonic, and supersonic jets. They found that upstream of the potential core, the low-rank decompositions were of compact wave-packet shape in the shear region of the jet; whereas downstream of the potential core, the modes were not low rank with many overlapping, spreadout modes with lower phase velocities. These two wave-packet types were named Kelvin–Helmholtz and Orr-type wave packets, respectively, due to their probable source mechanisms. The behaviors of groups 3, 4, and 5 (purple, green, and yellow) exemplify these same characteristics. The unidirectional radiation of group 3 (purple) would imply a low-rank wave packet of supersonic phase velocity, whereas the less directional radiation of groups 4 and 5 (green and yellow) would imply that only portions of the wave-number spectrum of the wave packets are in the supersonic regime, which agrees with groups 4 and 5 (green and yellow) originating farther downstream where convective velocities are lower. Bogey and Pineau [53] similarly observed in direct numerical simulations of temporally developing jets that the low-frequency aft radiation originates from the region just downstream of the potential core.

The differences between group 3 (purple) and groups 4 and 5 (green and yellow) are also observed when comparing two studies that use event-based inverse methods similar to the current work. Schlinker et al. [40] and Hileman and Samimy [28] used a similar cross-correlation beamforming method but with large-amplitude events as the triggers. For a full-scale engine at full power, Schlinker et al. [40] found the source locations along the jet axis to be concentrated at five diameters downstream, whereas Hileman and Samimy [28] found for a cold model-scale jet at three Mach numbers the peak in the distributions to be about 9–10 diameters downstream. Schlinker et al. [40] explains some of the differences are in part due to their placement of sensors at 135 deg relative to the nozzle, compared to 160 deg for Hileman and Samimy's [28] study. These results are corroborated in the current work, which possibly suggests that the sensor placement for Schlinker et al. [40] would measure events related to group 3 (purple) and Hileman and Samimy [28] to groups 4 and 5 (green and yellow). Furthermore, Schlinker et al. [40] also proposes that Hileman and Samimy's [28] distribution corresponds to the more dominant large-scale turbulent structure mechanisms at the end of the potential core rather than the Mach wave signature captured in their study.

VI. Conclusions

This paper has identified acoustic source regions along the nozzle lip line of a military aircraft that correspond to higher crackle percept [32,33] in the near field by an event-based beamforming method. Short-windowed segments of the waveform around 1000 of the highest derivative values are chosen as events in the beamforming process. Six distinct microphone pair groupings have been defined, with particular interest given to those that exceed the criterion for continuous crackle [groups 3–5 (purple, green, and yellow), $Sk\{\partial p/\partial t\} > 3$]. These three crackle-related groups propagate downstream but have differing source locations and directivities. Events beamformed from group 3 (purple) display unidirectional radiation and likely originate from the shear layer upstream of the collapse of the potential core, consistent with the description of Mach wave radiation [10]. Groups 4 and 5 (green and yellow) likely originate downstream of the potential core and appear similar to large-scale turbulent structure noise. Additional work needs to be undertaken to determine the relationship of these near-field shock events to far-field crackle perception and community response to jet crackle.

Appendix: Event Correlation and Statistics Tables of Beamforming Results

To correlate the windowed waveform segments one to another, the cross-correlation coefficient ρ_{xy} is calculated for each of the 1000
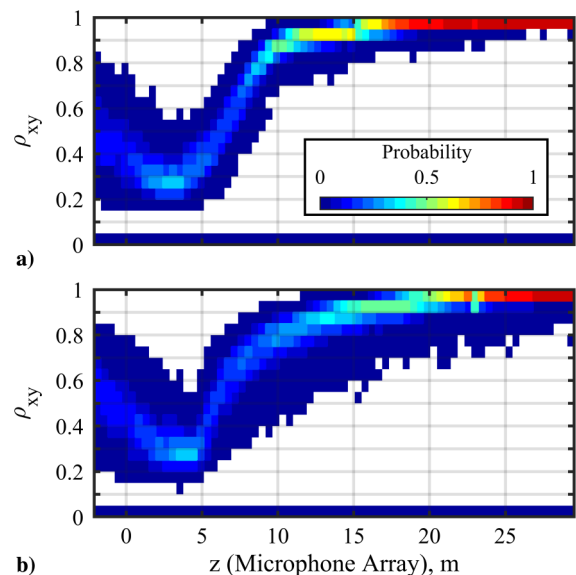

Fig. A1 **Normalized histograms of cross-correlation coefficient values for 1000 events from each microphone pair for a) 75 and b) 150% ETR.**

Table A1   Apparent jet lip-line origin 5th and 95th percentiles as well as mean μ of compiled grouping histograms across engine condition[a]

Group no.	Color	75% ETR			100% ETR			130% ETR			150% ETR		
		5th	μ	95th	5th	μ	95th	5th	μ	95th	5th	μ	95th
1	Blue	2.3	4.0	5.2	2.9	5.1	6.9	3.2	5.7	8.4	3.8	6.3	8.5
2	Red	0.9	3.3	9.1	1.4	4.5	7.6	1.3	4.9	9.1	1.1	5.6	8.8
3	Purple	–	–	–	2.0	4.3	6.0	2.3	5.3	7.3	2.5	7.0	9.7
4	Green	1.9	3.6	5.0	3.3	5.9	7.7	6.5	8.9	11.0	8.3	10.8	12.8
5	Yellow	2.8	5.5	7.9	3.3	6.2	8.6	5.1	8.6	12.2	7.5	11.0	14.6
6	Orange	–	–	–	–	–	–	–	–	–	6.5	9.6	12.8
Total	–	1.7	3.6	6.9	2.6	4.9	7.9	3.5	6.9	11.1	4.1	8.0	13.0

[a]A dash (–) notes groups that are not applicable for a given engine condition.

Table A2   Propagation angle 5th and 95th percentiles as well as mean μ of compiled grouping histograms across engine condition[a]

Group no.	Color	75% ETR			100% ETR			130% ETR			150% ETR		
		5th	μ	95th	5th	μ	95th	5th	μ	95th	5th	μ	95th
1	Blue	49.2	71.6	123.0	47.5	70.9	133.1	43.1	68.7	139.2	40.7	68.1	143.7
2	Red	86.5	112.0	126.3	78.9	106.8	122.4	70.6	103.6	125.5	66.4	103.5	146.0
3	Purple	–	–	–	118.9	124.4	131.3	110.4	115.6	122.0	108.8	114.4	122.2
4	Green	127.0	141.0	152.4	128.2	141.0	152.0	116.7	130.7	145.4	118.0	129.4	141.5
5	Yellow	150.6	153.3	156.9	149.0	152.5	156.3	140.5	149.1	155.3	132.7	142.9	150.8
6	Orange	–	–	–	–	–	–	–	–	–	145.9	150.1	154.2
Total	–	70.5	127.4	155.5	63.7	122.5	155.1	61.1	117.1	153.8	57.9	113.7	151.8

[a]A dash (–) notes groups that are not applicable for a given engine condition.

events in the 70 adjacent microphone pairs; and the resulting normalized histograms are given for 75 and 150% ETR in Fig. A1. The trend of ρ_{xy} for the individual events examined in this study follows a similar trend as the coherence length analysis for the same dataset performed by Leete et al. [50]. The lowest ρ_{xy} values are at microphones positioned 2–5 m downstream, which corresponds to the transition region from upstream to downstream radiation. On average, $\rho_{xy} \cong 0.5$ at $z = -2$ m (farthest upstream location), dips down to 0.3 at $z = 3$–5 m, and then increases nearly asymptotically toward one at the end of the array. The average ρ_{xy} is greater than 0.8 at $z > 9$ m for 75% ETR and at $z > 12$ m for 150% ETR. The other engine powers serve as intermediate cases with the same trends. The cross-correlation coefficients are greatest at far downstream locations, likely due in part to the orientation of the array allowing for the microphones to be more in line with the direction of radiation.

Statistic results for the event-based beamforming grouping analysis are noted in Tables A1 and A2. The 5th and 95th percentiles and the mean listed in Table A1 are shown graphically in Fig. 10 and correspond to the distributions given in Fig. 11. While the values in Table A2 are not graphically depicted, they add additional quantitative information that allow for further comparisons between microphone pair groups, as well as provide an opportunity for relative source distribution and directivity comparisons with other studies.

Acknowledgments

References

[1] Ffowcs Williams, J. E., Simson, J., and Virchis, V. J., "'Crackle': An Annoying Component of Jet Noise," *Journal of Fluid Mechanics*, Vol. 71, No. 2, 1975, pp. 251–271.
https://doi.org/10.1017/S0022112075002558

[2] Krothapalli, A., Venkatakrishnan, L., and Lourenco, L., "Crackle: A Dominant Component of Supersonic Jet Mixing Noise," AIAA Paper 2000-2024, June 2000.
https://doi.org/10.2514/6.2000-2024

[3] Gee, K. L., Neilsen, T. B., Muhlestein, M. B., Wall, A. T., Downing, J. M., James, M. M., and McKinley, R. L., "On the Evolution of Crackle

in Jet Noise from High-Performance Engines," AIAA Paper 2013-2190, June 2013.
https://doi.org/10.2514/6.2013-2190

[4] McInerny, S., Downing, M., Hobbs, C., James, M., and Hannon, M., "Metrics that Characterize Nonlinearity in Jet Noise," *AIP Conference Proceedings*, Vol. 838, No. 1, 2006, pp. 560–563.
https://doi.org/10.1063/1.2210418

[5] Fievet, R., Tinney, C. E., Baars, W. J., and Hamilton, M. F., "Coalescence in the Sound Field of a Laboratory-Scale Supersonic Jet," *AIAA Journal*, Vol. 54, No. 1, 2016, pp. 254–265.
https://doi.org/10.2514/1.J05452

[6] Mora, P., Heeb, N., Kastner, J., Gutmark, E. J., and Kailasanath, K., "Effect of Heat on the Pressure Skewness and Kurtosis in Supersonic Jets," *AIAA Journal*, Vol. 52, No. 4, 2014, pp. 777–787.
https://doi.org/10.2514/1.J052612

[7] Tam, C. K. W., Spyropoulos, J. T., Aubert, A. C., and Powers, R. W., "Crackle in the Noise of High-Performance Aircraft," AIAA Paper 2018-3306, June 2018.
https://doi.org/10.2514/6.2018-3306

[8] Pineau, P., and Bogey, C., "Steepened Mach Waves Near Supersonic Jets: Study of Azimuthal Structure and Generation Process Using Conditional Averages," *Journal of Fluid Mechanics*, Vol. 880, Oct. 2019, pp. 594–619.
https://doi.org/10.1017/jfm.2019.729

[9] Veltin, J., Day, B. J., and McLaughlin, D. K., "Correlation of Flowfield and Acoustic Field Measurements in High-Speed Jets," *AIAA Journal*, Vol. 49, No. 1, 2011, pp. 150–163.
https://doi.org/10.2514/1.J050583

[10] Murray, N. E., and Lyons, G. W., "On the Convection Velocity of Source Events Related to Supersonic Jet Crackle," *Journal of Fluid Mechanics*, Vol. 793, March 2016, pp. 477–503.
https://doi.org/10.1017/jfm.2016.127

[11] Gee, K. L., Sparrow, V. W., James, M. M., Downing, J. M., Hobs, C. M., Gabrielson, T. B., and Atchley, A. A., "The Role of Nonlinear Effects in the Propagation of Noise from High Power Aircraft," *Journal of the Acoustical Society of America*, Vol. 123, No. 6, 2008, pp. 4082–4093.
https://doi.org/10.1121/1.2903871

[12] Gee, K. L., Downing, J. M., James, M. M., McKinley, R. C., McKinley, R. L., Neilsen, T. B., and Wall, A. T., "Nonlinear Evolution of Noise from a Military Aircraft During Ground Run-Up," AIAA Paper 2012-2258, June 2012.
https://doi.org/10.2514/6.2012-2258

[13] Baars, W. J., Tinney, C. E., Wochner, M. S., and Hamilton, M. F., "On Cumulative Nonlinear Acoustic Waveform Distortions from

High-Speed Jets," *Journal of Fluid Mechanics*, Vol. 749, May 2014, pp. 331–366.
https://doi.org/10.1017/jfm.2014.228

[14] Murray, N. E., and Baars, W. J., "Passive Nozzle-Based Technology for Reduction of Heated Supersonic Jet Noise," AIAA Paper 2019-2729, May 2019.
https://doi.org/10.2514/6.2019-2729

[15] Daniel, K., Mayo, D., Jr., Lowe, K. T., and Ng, W. F., "Experimental Investigation of the Pressure Field of a Heated Supersonic Jet with a Centered Total Temperature Non-Uniformity," AIAA Paper 2018-3145, June 2018.
https://doi.org/10.25/6.2018-3145

[16] Martens, S., Spyropoulos, J. T., and Nagel, Z., "The Effect of Chevrons on Crackle—Engine and Scale Model Results," *ASME Turbo Expo 2011*, American Soc. of Mechanical Engineers Paper GT2011-46417, Fairfield, NJ, 2011, pp. 315–326.
https://doi.org/10.1115/GT2011-46417

[17] Papamoschou, D., and Debiasi, M., "Directional Suppression of Noise from a High-Speed Jet," *AIAA Journal*, Vol. 39, No. 3, 2001, pp. 380–387.
https://doi.org/10.2514/2.1345

[18] Chen, S., and Mihaescu, M., "Nozzle Pressure Ratio Effects on Aerodynamics and Acoustics of a Highly-Heated Rectangular Supersonic Jet," AIAA Paper 2019-2753, May 2019.
https://doi.org/10.2514/6.2019-2753

[19] Buchta, D. A., Anderson, A. T., and Freund, J. B., "Near-Field Shocks Radiated by High-Speed Free-Shear Flow Turbulence," AIAA Paper 2014-3201, June 2014.
https://doi.org/10.2514/6.2014-3201

[20] Anderson, A. T., and Freund, J. B., "Source Mechanisms of Jet Crackle," AIAA Paper 2012-2251, June 2012.
https://doi.org/10.2514/6.2012-2251

[21] Pineau, P., and Bogey, C., "Temperature Effects on Convection Speed and Steepened Waves of Temporally Developing Supersonic Jets," *AIAA Journal*, Vol. 58, No. 3, 2020, pp. 1227–1239.
https://doi.org/10.2514/1.J058589

[22] Nichols, J. W., Lele, S. K., Ham, F. E., Martens, S., and Spyropoulos, J. T., "Crackle Noise in Heated Supersonic Jets," *Journal of Engineering for Gas Turbines and Power*, Vol. 135, No. 5, April 2013, Paper 051202.
https://doi.org/10.1115/1.4007867

[23] Nichols, J. W., Lele, S. K., and Spyropoulos, J. T., "The Source of Crackle Noise in Heated Supersonic Jets," AIAA Paper 2013-2197, June 2013.
https://doi.org/10.2514/6.2013-2197

[24] Chen, S., Gojon, R., and Mihaescu, M., "High-Temperature Effects on Aerodynamic and Acoustics Characteristics of a Rectangular Supersonic Jet," AIAA Paper 2018-3303, June 2018.
https://doi.org/10.2514/6.2018-3303

[25] Langenais, A., Vuillot, F., Troyes, J., and Bailly, C., "Accurate Simulation of the Noise Generated by a Hot Supersonic Jet Including the Turbulence Tripping and Nonlinear Acoustic Propagation," *Physics of Fluid*, Vol. 31, No. 1, 2019, Paper 01605.
https://doi.org/10.1063/1.5050905

[26] Laufer, J., Schlinker, R., and Kaplan, R. E., "Experiments on Supersonic Jet Noise," *AIAA Journal* Vol. 14, No. 4, April 1976, pp. 489–497.
https://doi.org/10.2514/3.61388

[27] Schlinker, R. H., Simonich, J. C., Reba, R. A., Colonius, T., and Ladeinde, F., "Decomposition of High Speed Jet Noise: Source Characteristics and Propagation Effects," AIAA Paper 2008-2890, May 2008.
https://doi.org/10.2514/6.2008-2890

[28] Hileman, J. I., and Samimy, M., "Mach Number Effects on Jet Noise Sources and Radiation to Shallow Angles," *AIAA Journal*, Vol. 44, No. 8, Aug. 2006.
https://doi.org/10.2514/1.19959

[29] Hileman, J., Thurow, B., and Samimy, M., "Development and Evaluation of a 3-D Microphone Array Locate Individual Acoustic Sources in a High-Speed Jet," *Journal of Sound and Vibration*, Vol. 276, Nos. 3–5, 2004, pp. 649–669.
https://doi.org/10.1016/j.jsv.2003.08.022

[30] Gee, K. L., Sparrow, V. W., Atchley, A. A., and Gabrielson, T. B., "On the Perception of Crackle in High-Amplitude Jet Noise," *AIAA Journal*, Vol. 45, No. 3, 2007, pp. 593–658.
https://doi.org/10.2514/1.26484

[31] Swift, S. H., Gee, K. L., and Neilsen, T. B., "Testing Two Crackle Criteria Using Modified Jet Noise Waveforms," *Journal of the Acoustical Society of America*, Vol. 141, No. 6, 2017, pp. EL549–EL554.
https://doi.org/10.1121/1.4984819

[32] Gee, K. L., Russavage, P. B., Neilsen, T. B., Swift, S. H., and Vaughn, A. B., "Subjective Rating of the Jet Noise Crackle Percept," *Journal of the Acoustical Society of America*, Vol. 144, No. 1, 2018, pp. EL40–EL45.
https://doi.org/10.1121/1.5046094

[33] Russavage, P. B., Neilsen, T. B., Gee, K. L., and Swift, S. H., "Rating the Perception of Jet Noise Crackle," *Proceedings of Meetings on Acoustics*, Vol. 33, No. 1, 2018, Paper 040001.
https://doi.org/10.1121/2.0000821

[34] James, M. M., Salton, A. R., Downing, J. M., Gee, K. L., Neilsen, T. B., Reichman, B. O., McKinley, R. L., Wall, A. T., and Gallagher, H. L., "Acoustic Emissions from F-35B Aircraft During Ground Run-Up," AIAA Paper 2015-2375, June 2015.
https://doi.org/10.2514/6.2015-2375

[35] Wall, A. T., Leete, K. M., Gee, K. L., Neilsen, T. B., James, M. M., and McKinley, R. L., "Preliminary Investigation of Multilobe Fighter Jet Noise Sources Using Acoustical Holography," AIAA Paper 2017-3520, June 2017.
https://doi.org/10.2514/6.2017-3520

[36] Swift, S. H., Gee, K. L., Neilsen, T. B., Wall, A. T., Downing, J. M., and James, M. M., "Spatiotemporal Correlation Analysis of Jet Noise from a Round-Nozzle Supersonic Aircraft," AIAA Paper 2018-3938, June 2018.
https://doi.org/10.2514/6.2018-3938

[37] Neilsen, T. B., Vaughn, A. B., Gee, K. L., Swift, S. H., Wall, A. T., Downing, J. M., and James, M. M., "Three-Way Spectral Decompositions of High-Performance Military Aircraft Noise," *AIAA Journal* Vol. 57, No. 8, May 2019, pp. 3467–3479.
https://doi.org/10.2514/1.J057992

[38] Leete, K. M., Wall, A. T., Gee, K. L., Neilsen, T. B., James, M. M., and Downing, J. M., "Dependence of High-Performance Military Aircraft Noise on Frequency and Engine Power," AIAA Paper 2018-2826, June 2018.
https://doi.org/10.2514/6.2018-2826

[39] Vaughn, A. B., Gee, K. L., Swift, S. H., Wall, A. T., Downing, J. M., and James, M. M., "Beamforming of Supersonic Jet Noise for Crackle-Related Events," *Proceedings of Meetings on Acoustics*, Vol. 35, No. 1, 2018, Paper 040003.
https://doi.org/10.1121/2.0000998

[40] Schlinker, R. H., Liljenberg, S. A., Polak, D. R., Post, K. A., Chipman, C. T., and Stern, A. M., "Supersonic Jet Noise Source Characteristics and Propagation: Engine and Model Scale," AIAA Paper 2007-3623, June 2007.
https://doi.org/10.2514/6.2007-3623

[41] Vaughn, A. B., "Physical Characterization of Crackle-Related Events in Military Jet Aircraft Noise," M.S. Thesis, Brigham Young Univ., Provo, UT, 2020.

[42] Bendat, J. S., and Piersol, A. G., "Stationary Random Processes," *Random Data Analysis and Measurement Procedures*, 4th ed. Vol. 1, Wiley, New York, 2010, pp. 116–118.

[43] Gee, K. L., Neilsen, T. B., Wall, A. T., Downing, J. M., James, M. M., and McKinley, R. L., "Propagation of Crackle-Containing Jet Noise from High-Performance Engines," *Noise Control Engineering Journal*, Vol. 64, No. 1, 2016, pp. 1–12.
https://doi.org/10.3397/1/376354

[44] Karzova, M. M., Lechat, T., Ollivier, S., Dragna, D., Yuldashev, P. V., Khokhlova, V. A., and Blanc-Benon, P., "Effect of Surface Roughness on Nonlinear Reflection of Weak Shock Waves," *Journal of the Acoustical Society of America*, Vol. 146, No. 5, 2019, pp. EL438–EL443.

[45] Marchiano, R., Coulouvrat, F., Baskar, S., and Thomas, J. L., "Experimental Evidence of Deviation from Mirror Reflection for Acoustical Shock Waves," *Physical Review E*, Vol. 76, No. 5, 2007, Paper 056602.
https://doi.org/10.1103/PhysRevE.760566602

[46] Stout, T. A., Gee, K. L., Neilsen, T. B., Wall, A. T., and James, M. M., "Source Characterization of Full-Scale Jet Noise Using Acoustic Intensity," *Noise Control Engineering Journal*, Vol. 63, No. 6, 2015, pp. 522–536.
https://doi.org/10.3397/1/376346

[47] Nagamatsu, H. T., and Horvay, G., "Supersonic Jet Noise," AIAA Paper 1970-0237, Jan. 1970.
https://doi.org/10.2514/6.1970-237

[48] Panda, J., Seaholtz, R. G., and Elam, K. A., "Investigation of Noise Sources in High-Speed Jets via Correlation Measurements," *Journal of Fluid Mechanics*, Vol. 537, Aug. 2005, pp. 349–385.
https://doi.org/10.1017/S0022112005005148

[49] Tam, C. K. W., Viswanathan, K., Ahuja, K. K., and Panda, J., "The Sources of Jet Noise: Experimental Evidence," *Journal of Fluid Mechanics*, Vol. 615, Nov. 2008, pp. 254–292.
https://doi.org/10.1017/S0022112008003704

[50] Leete, K. M., Gee, K. L., Liu, J., and Wall, A. T., "Coherences Analysis of the Noise from a Simulated Highly-Heated Laboratory-Scale Jet," *AIAA Journal*, Vol. 58, No. 8, May 2020, pp. 3426–3435.
https://doi.org/10.2514/1.J059112

[51] Tam, C. K. W., and Auriault, L., "Jet Mixing Noise from Fine-Scale Turbulence," *AIAA Journal*, Vol. 37, No. 2, Feb. 1999, pp. 145–153.
https://doi.org/10.2514/2.691

[52] Schmidt, O. T., and Schmid, P. J., "A Conditional Space-Time POD Formalism for Intermittent and Rare Events: Example of Acoustic Bursts in Turbulent Jets," *Journal of Fluid Mechanics*, Vol. 867, May 2019, Paper R2.
https://doi.org/10.1017/jfm.2019.200

[53] Bogey, C., and Pineau, P., "Potential-Core Closing of Temporally Developing Jets at Mach Numbers Between 0.3 and 2: Scaling and Conditional Averaging of Flow and Sound Fields," *Physical Review Fluids*, Vol. 4, No. 12, Dec. 2019, Paper 124601.
https://doi.org/10.1103/PhysRevFluids.4.124601

D. Papamoschou
Associate Editor